Numerical Contact Model of a Smooth Ball on an Anisotropic Rough Surface

C. Y. Poon

R. S. Sayles

Department of Mechanical Engineering,
Imperial College,
London SW7 2AZ, UK

A numerical elastic-plastic contact model of a smooth ball on a directionally structured anisotropic rough surface is presented. The contact model is tested on three types of surface contact of a smooth ball on (i) a smooth surface, (ii) a sinusoidal surface, and (iii) a real rough surface. The validity of the model is proven by good agreement of the numerical result for the smooth surface with the Hertz analytical result. The contact of the sinusoidal surface shows that by the introduction of surface undulation in a regular pattern, the real pressure distribution follows the expected behavior where the contact pressure at the peak is maximum and the contact pressure at the valley is zero and the peak pressure decreases away from the ball center. The contact of the real rough surface shows the ability of the model to cope with the more practically realistic situation where the asperity heights are distributed randomly. The results of the rough surface contact analysis for different surface roughness are presented in a separate paper.

1 Introduction

It is understood that when two surfaces are brought together surface roughness causes contact to occur at discrete contact spots. The actual area of contact of microscopically rough surfaces and the changes that occur under load and relative motion are the important parameters in understanding many tribological phenomena, such as stiffness of joints, wear, adhesion, friction force, frictional heating, thermal and electrical contact resistance and fluid leakage. The real contact area can be obtained by (i) experimental techniques, (ii) stochastic approach, and (iii) numerical contact model.

In the experimental approach, the methods reported are thermal and electrical conduction (Bowden and Tabor, 1950; Holm, 1958), optical direct observation (Holm, 1958; Dyson and Hirst, 1954; Kragelskii, 1965), internal reflection (Kragelskii and Demkin, 1960), Nomarski interferometry (Uppal et al., 1972); Neutrographical method (Johannet, 1972), computer simulation (Williamson, 1967/68; Sayles, 1978b), relocation profilometry (Williamson and Hunt, 1968; Uppal and Probert, 1973).

The realization that surface asperity heights can often be regarded as possessing a Gaussian distribution has drawn attention to the use of random process theory as a means of deriving of the load-area relationship. Greenwood and Williamson (1966) were among the first to take into account the statistical nature of the asperity distribution on surfaces. Other workers, e.g., Tsukizoe and Hisakado (1965, 1968), Onions and Archard (1973), Mikic and Roca (1974), Bush and Gibson (1975), used the similar approach to derive the interfacial force and contact area as a function of separation from the mean line. Other workers (Bush et al., 1975, 1978; Suratkar et al., 1976) have approached the problem with more mathematically complex random process models following the work of Longuet-Higgins (1957a, 1957b) and Nayak (1971), for plastic and elastic contact.

Over the last few years, numerical techniques (Francis, 1982, 1983; Chiu and Liu, 1970; Webster and Sayles, 1986a; West et al., 1987a; West and Sayles, 1987b) have been developed and used on rough surface contact problems. This approach provides a deterministic solution to rough surface contact stresses and areas for the approach does not require an asperity model and makes no probabilistic assumptions such as the distribution of asperity heights, slopes, curvatures. The technique takes full account of the interaction of deformation from all the contact points and highlights the deformable contact geometry of rough surfaces under loading. It provides useful information on the number of contacts, their sizes and distributions, and the spacing between contacts.

In this paper, a numerical elastic-plastic contact model of a smooth ball on a directionally structured anisotropic rough surface is presented. This type of contact geometry is found commonly in many engineering applications such as the contact of a ball on the countersurface of ball bearings, ball screws, spherical bearings, ball joints etc, in which the surfaces are produced by grinding. The contact model is directly relevant to the work reported by Hirst and Hollander (1974) and Poon (1989). In their experimental work, a smooth ball was slid on a directionally structured anisotropic and normally flat rough surface. The surface damage was found to be related to the surface parameters σ and β^*, where σ is the root-mean-square (rms) of the height distribution and β^* is the correlation length describing the spatial variation of surface height. It is important to understand the surface contact mechanics in an attempt

Contributed by the Tribology Division for publication in the JOURNAL OF TRIBOLOGY. Manuscript received by the Tribology Division January 14, 1993; revised manuscript received May 10, 1993. Associate Technical Editor: C. Cusano.

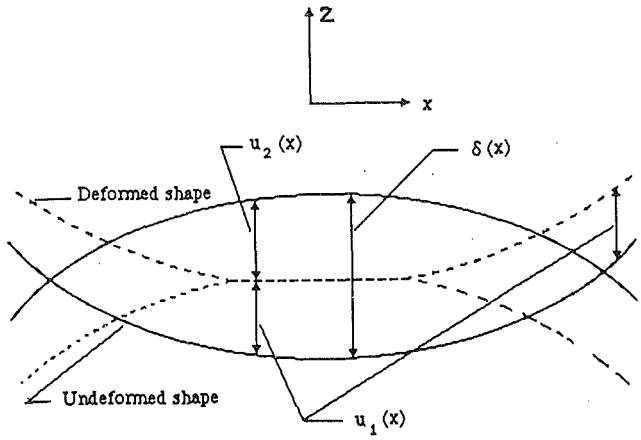

Fig. 1 Diagram showing the geometric overlap and deformed shape of an ideal smooth contact

to reveal the mechanistic processes influencing the sliding friction and surface damage. The model has been used to obtain the contact information such as the extent of plastic deformation and the states of contact over a range of rough surfaces and results from the analysis have been used to correlate results from friction tests (Poon, 1989). Furthermore, the model has also been applied to study the effects of surface roughness and waviness upon the real contact area, spacings and asperity contact pressures. The results are presented in a separate paper.

2 Constraints of the Numerical Contact Model

Referring to Fig. 1 and in addition to the usual linear elastic theory assumptions, the assumptions of the model are:

(1) Strains are sufficiently small for the linear elastic theory equations to be applicable.

(2) The contact area is contained within the geometric overlap region.

(3) Inside the elastic contact region, the total displacement, δ, is equal to the sum of the displacements of each body, u_1 and u_2, i.e., $u_1(x)+u_2(x)=\delta(x)$ for $H>p(x)>0$ where H is the Hardness of the softer material.

(4) Inside the plastic contact region, the pressure is equal to H.

(5) Outside the contact region,

$$u_1(x)+u_2(x)>\delta(x) \quad \text{and} \quad p(x)=0$$

(6) Relative horizontal strains and displacements are ignored, i.e., contact is frictionless.

(7) The surface slopes are reasonably small so that forces can be assumed to act normally to the surfaces.

3 The Plasticity Model

The plasticity model used is based on the experimental observations of Samuels and Mulhearn (1956) and Mulhearn (1959) that the subsurface displacements produced by any blunt indenter are approximately radial from the point of first contact, with roughly hemispherical contours of equal strain. The plastic zone is contained within the interior of the body and the material displaced by plastic flow can be considered to be accommodated by the elastic expansion of the subsurface core (see Johnson's "cavity" model of mixed elastic-plastic deformation (Johnson, 1985)). In the contact model, the contact pressure is allowed to increase until it is equal to the hardness of the softer material.

4 Contact Equations

The classical approach to finding the stresses and displacements in an elastic half-space due to surface forces is due to Boussinesq (1885), and Cerruti (1882) who made use of the theory of potential. The approach is presented by Love (1952). The Boussinesq theory gives the normal surface deflection u_z of a surface point due to a concentrated point force P_L acting at a distance r normally to the surface, i.e.,

$$u_z=\frac{1-v^2}{\pi E}\frac{P_L}{r} \tag{1}$$

The surface displacement produced by a normal pressure distributed over an area S of the surface can be obtained by superposition. A distributed pressure $p(r, \phi)$ in polar coordinates acting on the surface area S is equivalent to a force of magnitude $p\,r\,dr\,d\phi$. From Eq. (1), writing $P_L=p\,r\,dr\,d\phi$, the surface displacement due to $p(r, \phi)$ over an area S can be written as,

$$u_z=\frac{1-v^2}{\pi E}\int_S\int p(r, \phi)dr\,d\phi \tag{2}$$

The surface data is obtained by sampling on a rectangular grid over a finite interval. It is thus convenient to use a rectangular area of sides $2a\times 2b$ over which the normal pressure could be assumed uniform.

The effect of uniform pressure acting on a rectangular area of $2a\times 2b$ has been analyzed by Love (1929) using Eq. (2). The deflection of a general point (x, y) on the surface due to a uniform pressure p over a rectangle centered at the origin is:

$$\begin{aligned}\frac{\pi E}{1-v^2}\frac{u_z}{p}=&(x+a)\ln\left[\frac{(y+b)+\{(y+b)^2+(x+a)^2\}^{1/2}}{(y-b)+\{(y-b)^2+(x+a)^2\}^{1/2}}\right]\\&+(y+b)\ln\left[\frac{(x+a)+\{(y+b)^2+(x+a)^2\}^{1/2}}{(x-a)+\{(y+b)^2+(x-a)^2\}^{1/2}}\right]\\&+(x-a)\ln\left[\frac{(y-b)+\{(y-b)^2+(x-a)^2\}^{1/2}}{(y+b)+\{(y+b)^2+(x-a)^2\}^{1/2}}\right]\\&+(y-b)\ln\left[\frac{(x-a)+\{(y-b)^2+(x-a)^2\}^{1/2}}{(x+a)+\{(y-b)^2+(x+a)^2\}^{1/2}}\right]\end{aligned} \tag{3}$$

Equation (3) gives the exact solution of a surface deflection due to the uniform pressure acting on a rectangular area. If the distance between the surface deflection and the elemental pressure is large, Eq. (1) can be used as a good approximation to relate the surface deflection and the pressure. In this case, the concentrated load is simply equal to the pressure times the area. It is advantageous to use Eq. (1) in order to speed up the computing process. It has been shown (Poon, 1990) that if the surface deflection is outside the pressure acting on the rectangular area $2a\times 2b$, Eq. (1) can be used to relate the surface deflection and the pressure with accuracy up to 95 percent.

The total deflection at any point is calculating by summing the influence of each pressure element acting on area $2a\times 2b$. Therefore, we have a set of linear equations

$$[u_i]=[C_{ij}][p_j] \tag{4}$$

The values of the u_i's are obtained by giving the bodies a known bulk overlap. The sum of the strains in the two bodies at any contacting point is equal to the geometric overlap δ. Thus, the strain in each body can be expressed in terms of the geometric overlap using the relationship:

$$\frac{u_{z1}E_1}{1-v_1^2}=\frac{u_{z2}E_2}{1-v_2^2} \tag{5}$$

which gives

$$u_{z1}=\frac{\delta}{1+\dfrac{E_1(1-v_2^2)}{E_2(1-v_1^2)}} \tag{6}$$

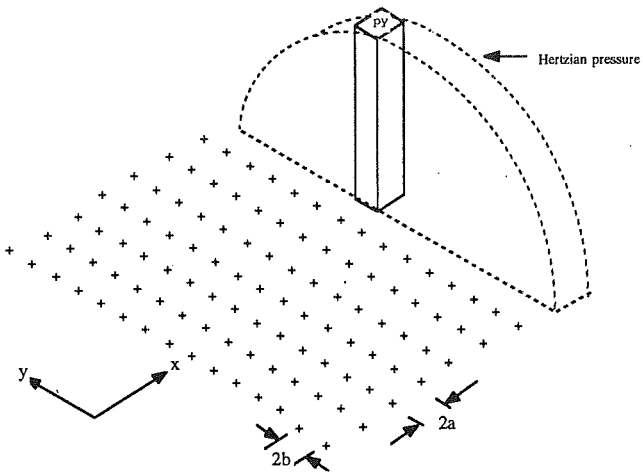

Fig. 2 Schematic representation of surface and pressure elements

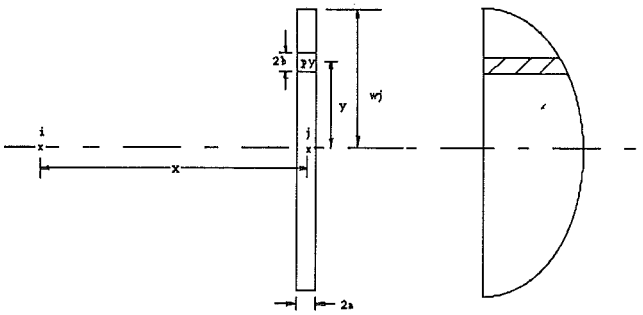

Fig. 3 Diagram showing the surface displacement *i* and pressure element p_y subdivided by Hertzian pressure at *j*.

By assuming some of the points to be in contact, the strains at these points of contact can be obtained. The influence coefficients can be calculated by using Eq. (1) or (3) depending on the distance between the pressure element and the surface point. The solution of the set of simultaneous equations is obtained by the Gaussian Back Elimination method.

Once the solution for the elemental pressures has been found by elemental pressures which are negative are removed from the contact (Assumption 5). Also, any asperity with a calculated pressure greater than the flow pressure would collapse and the pressure should be reduced to the flow pressure. There are two methods to reduce the pressure. The first method is to allow the asperity to collapse by modifying the shape of the original undeformed surfaces until the pressures are equal to the flow pressure of the material. The second method is to put the presures equal to the flow pressure and re-calculate the pressure distribution until all pressures satisfy the contact conditions. In the numerical solution employed here, the second method is used, as it gives a direct method of obtaining the plastic area and no assumption of the asperity shape is needed.

The deformations are then found everywhere to check that no contact occurs outside the assumed contact regions. If contact does occur outside these regions, the extra points are added to the assumed contact region and the system of linear equations is then solved again for the new assumed contact points.

This process is repeated until convergence on a particular set of contact points is achieved. The total contact area, the plastic area and the normal load can then be calculated by integrating the contact elements and their pressures.

5 Numerical Solution

The methods described in Section 4 can be applied to calculate the contact pressures of any two contacting bodies with different geometries for general three dimensional contact problems. In some particular cases, the contact solution can be reduced to two dimensional by appropriate modifications and assumptions. In the following, the numerical solution of a smooth ball on an ansiotropic rough surface in two dimensional contact is described.

In the contact model, referring to Fig. 2, the surface height is assumed to vary only in the x-direction and have the same height value in the y-direction. The contact pressure of each element is further assumed Hertzian in the y-direction. In the numerical solution, the surface deflections and the contact pressures at $y=0$ are determined. In Fig. 2, the pressure p_y along the y-direction for an element j is,

$$p_y = p_j\left(1-\frac{y^2}{w_j^2}\right)^{1/2} \tag{7}$$

where w_j is the contact length from the center.

Referring to Fig. 3, showing a uniform pressure element p_y acting on an elemental area $2a\times 2b$, the vertical surface displacements at point i due to an applied pressure p_y is given by Eq. (1) or (3), thus we have

$$u_i = p_y\frac{(1-v^2)}{\pi E}F_{xy} \tag{8}$$

where

$$F_{xy}=\frac{2a\cdot 2b}{\sqrt{x^2+y^2}} \tag{9}$$

or

$$\begin{aligned}F_{xy} = {} & (x+a)\ln\left[\frac{(y+b)+\{(y+b)^2+(x+a)^2\}^{1/2}}{(y-b)+\{(y-b)^2+(x+a)^2\}^{1/2}}\right]\\ & +(y+b)\ln\left[\frac{(x+a)+\{(y+b)^2+(x+a)^2\}^{1/2}}{(x-a)+\{(y+b)^2+(x-a)^2\}^{1/2}}\right]\\ & +(x-a)\ln\left[\frac{(y-b)+\{(y-b)^2+(x-a)^2\}^{1/2}}{(y+b)+\{(y+b)^2+(x-a)^2\}^{1/2}}\right]\\ & +(y-b)\ln\left[\frac{(x-a)+\{(y-b)^2+(x-a)^2\}^{1/2}}{(x+a)+\{(y-b)^2+(x+a)^2\}^{1/2}}\right]\end{aligned} \tag{10}$$

For each element j, the pressure is subdivided into $2Ny+1$ elements. The elemental width $2b$ is given by,

$$2b=\frac{2w_j}{2N_y+1} \tag{11}$$

The distance between elements i and j is given by,

$$x=|i-j|\cdot 2a \tag{12}$$

Writing $y=k\cdot 2b$, the surface displacement at point i due to Hertzian pressure at j becomes,

$$u_i=\frac{1-v^2}{\pi E}\sum_k p_j\left(1-\frac{4k^2}{(2N_y+1)^2}\right)^{1/2}\cdot F_{xy} \tag{13}$$

where $k=0,\ \pm 1,\ \pm 2,\ \ldots,\ \pm Ny$

If the number of contacts is N_c, then a set of simultaneous equations can be set up by superposition. Thus,

$$[u_i]=[C_{ij}][p_j] \tag{14}$$

where i and $j=1,\ 2,\ 3,\ \ldots N_c$ or

$$u_i=\frac{1-v^2}{\pi E}\sum_j\sum_k p_j\left(1-\frac{4k^2}{(2N_y+1)^2}\right)^{1/2}\cdot F_{xy} \tag{15}$$

The set of simultaneous Eqs. (14) are solved by a Matrix Inversion method. An initial guess of the contacting points can be obtained by considering the regions of geometrical overlap between the two bodies. For each point in contact, the strain in each body is calculated using Eq. (6).

If the contact length of each element, in the y direction, is

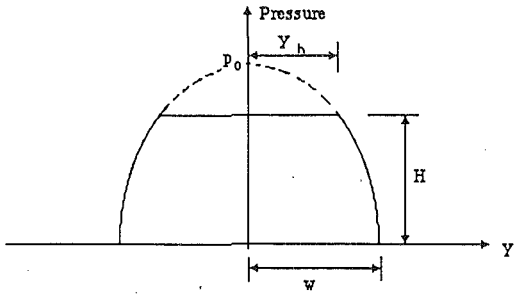

Fig. 4 Diagram showing the elastic pressure being truncated to give the plastic pressure profile

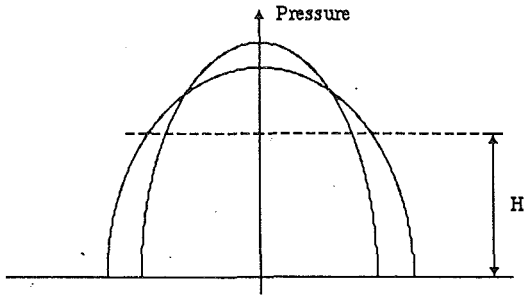

Fig. 5 Diagram showing two possible forms of Hertzian pressure having the same asperity load

known, then the influence coefficient can be calculated and the contact pressure found. The determination can be obtained by the information given at the boundary of contact at which the surface deflection u_i given by Eq. (6) is equal to the surface deflection u_z induced by the contact pressures. If $u_z > u_i$, then the contact length is overestimated and the contact length should be reduced. Similarly, if $u_z < u_i$, the contact length should be increased. However, there is no direct method relating contact lengths to surface deflections or pressures, and therefore no direct method of defining an appropriate change to the contact lengths. An effective way to determine the contact lengths will be discussed later.

The initial contact lengths are obtained by the geometrical overlap which allows a calculation of the first set of p_j's. If there are negative elemental pressures, these points are excluded and the problem solved again to obtain a new set of C_{ij}'s and p_j's. This process is repeated until the values of the p_j's are everywhere positive.

The next step is to compare the values of elastic pressure p_j to the material hardness H. If any elemental pressure is greater than H, the point of displacement is shifted from the center of the contact element where plastic flow will begin to a point where the contact pressure begins to decrease. An index array is used to store the plastic contact width p_{cw}. The plastic contact width is incremented according to the difference of the current p_j's and H. In the case of plastic deformation, the pressure profile is no longer Hertzian and Eq. (13) has to be modified to include the effect of plastic deformation. Consider the Hertzian pressure profile being truncated to give the pressure profile under plastic deformation shown in Fig. 4. When $y < y_h$, the pressure will be equal to the indentation hardness H. On the other hand, when $y > y_h$ the pressure will be,

$$p = p_0\left(1 - \frac{y^2}{w_j}\right)^{1/2} \tag{16}$$

At $y = y_h$, $p = H$ thus eliminating p_0 from Eq. (16). Therefore,

$$p = H \cdot \sqrt{\left(1 - \frac{y^2}{w_j^2}\right) \Big/ \left(1 - \frac{y_h^2}{w_j^2}\right)} \quad \text{where } y > y_h \tag{17}$$

Writing y and y_h in terms of discrete points, i.e.,

$$y = k \cdot 2b \quad \text{where } k = 0, \pm 1, \pm 2, \ldots \pm N_k \tag{18}$$

and

$$y_h = k_h \cdot 2b \tag{19}$$

where k_h is the index of the point at which $y = y_h$. Substitute Eqs. (11), (18), and (19) into Eq. (17),

$$p = H \cdot \alpha_k \tag{20}$$

where

$$\alpha_k = \sqrt{(1 - \mu^2 k^2)/(1 - \mu^2 k_h^2)} \tag{21}$$

and

$$\mu = \frac{2}{2N_y + 1} \tag{22}$$

Thus, the elastic-plastic contact equations can be generalized as follows,

$$u_i = \frac{1 - v^2}{\pi E} \sum_k p_j \alpha_k F_{xy} \tag{23}$$

For elastic deformation, α_k is calculated by putting y_h equal to zero, which is Eq. (13). For plastic deformation, $p_j = H$. If $k < k_h$, α_k is equal to 1 and if $k > k_h$, α_k is given by Eq. (21). A set of C_{ij}'s are again obtained using Eq. (23). The solution for the p_j's is continued until the plasticity model is satisfied.

In what follows, the method of determining contact lengths is described. The contact lengths are always less than their geometrical overlap because of the pressure acting at the neighboring points. The amount of deformation depends upon the magnitude and the spatial distance of elemental pressures. At some stages of the iterative process, a change in contact length of a particular contact will redistribute the contact pressures which in turn will affect the displacements. In order to obtain an effective way to make changes to the previously assumed contact lengths, it is essential to know how the u_i's and p_j's vary with respect to the contact length w_j. A way of doing this is to differentiate Eq. (1) or (3) with respect to w_j. As far as the contact length at the boundary is concerned, Eq. (1) can be used as a good approximation. By differentiating Eq. (1) with respect to w_j, see Appendix,

$$\frac{du_i}{dw_j} = \frac{2a(1 - v^2)}{\pi E} \sum_j p_j \sum_k \alpha_k \frac{\mu x^2}{(x^2 + y^2)^{3/2}} + \frac{2a(1 - v^2)}{\pi E} \sum_j \frac{dp_j}{dw_j} \sum_k \alpha_k \frac{\mu w_j}{(x^2 + y^2)^{1/2}} \tag{24}$$

At equilibrium, the load capacity on each asperity is constant. Therefore, the change in contact length and pressure with respect to w_j will be in such a way that the load remains unchanged. The load L on each asperity with pressure p_j is given by,

$$L = 2 \cdot a \cdot \int_{-w_j}^{w_j} p_j \left(1 - \frac{y^2}{w_j^2}\right)^{1/2} \Big/ \left(1 - \frac{y_h^2}{w_j^2}\right)^{1/2} dy \tag{25}$$

writing

$$\theta = \sin^{-1}\frac{y_h}{w_j} \tag{26}$$

and solving Eq. (26)

$$L = 4 \cdot a - p_j \cdot \left(\frac{w_j \cdot \left(\frac{\pi}{2} - \theta - \frac{\sin 2\theta}{2}\right)}{\cos\theta} + y_h\right)$$

$$= 4 \cdot a \cdot p_j \cdot (w_j f + y_h) \tag{27}$$

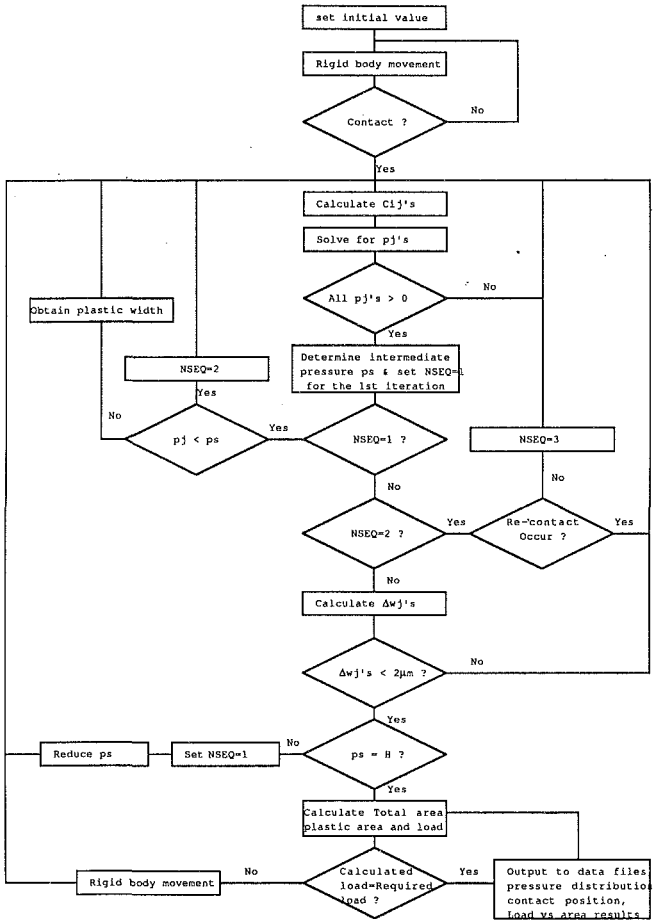

Fig. 6 Flow chart for the numerical elastic-plastic contact programs

where

$$f=\frac{\pi/2-\theta-\sin 2\theta/2}{\cos\theta} \tag{28}$$

Differentiating Eq. (28) with respect to w_j and putting $dL=0$, we get

$$\frac{dp_j}{dw_j}=\frac{-p_j}{w_j f+y_h}\left[\frac{y_h}{w_j}\left(2-\frac{f\sin\theta}{\cos^2\theta}\right)+f\right] \tag{29}$$

Substituting Eq. (29) into Eq. (24)

$$\frac{du_i}{dw_j}=\frac{2a(1-v^2)}{\pi E}\left[\sum_j p_j\sum_k\frac{\alpha_k\mu x^2}{(x^2+y^2)^{3/2}}\right]+\frac{2a(1-v^2)}{\pi E}\sum_j\frac{-p_j}{w_j f+y_h}\left[\frac{y_h}{w_j}\left(2-\frac{f\sin\theta}{\cos^2\theta}\right)+f\right]\times\sum_k\frac{\mu w_j}{(x^2+y^2)^{1/2}} \tag{30}$$

Thus, for small increments of surface displacement, we have a set of simultaneous equations

$$[\Delta u_i]=[A_{ij}][\Delta w_j] \tag{31}$$

where

$$A_{ij}=\frac{2a(1-v^2)}{\pi E}\left[\sum_j p_j\sum_k\frac{\alpha_k\mu x^2}{(x^2+y^2)^{3/2}}\right)+\frac{2a(1-v^2)}{\pi E}\sum_j\frac{-p_j}{w_j f+y_h}\left[\frac{y_h}{w_j}\left(2-\frac{f\sin\theta}{\cos^2\theta}\right)+f\right]\sum_k\frac{\mu w_j}{(x^2+y^2)^{1/2}} \tag{32}$$

At the boundary of contact the displacement u_i should be equal to the total surface deflection u_z induced by the contact pressure. If $u_z>u_i$, then the contact length is overestimated initially and the contact length should be reduced. Similarly, if $u_z\le u_i$, the contact length should be increased. Thus,

$$\Delta u_i=u_i-u_z \tag{33}$$

The terms A_{ij} can be obtained by the current values of p_j's and w_j's. A set of Δw_j's are obtained by solving the set of simultaneous Eqs. (31). A new set of contact lengths are established by adding the current values of contact lengths to the Δw_j's. The process of getting the w_j's and Δw_j's are repeated until all the values of Δw_j are smaller than an acceptable value, say 2 percent of the contact length in the y-direction.

Finally, the surface points out of contact are checked everywhere such that the surface displacements are greater than the geometrical overlap. Otherwise, the iterative process is repeated to obtain p_j's and w_j's with the points included in the contacts.

It may be noted that numerical contact solution involves many unknowns such as the number of contacts, the contact lengths and the plastic lengths, each affecting the other. Initially, the geometrical overlap length w_g is used to obtain the pressure distribution. The actual contact length w_a is always less than the geometrical overlap resulting in the underestimation of pressure. Figure 5 shows two possible forms of Hertzian pressure having the same asperity load but with different contact lengths. If both the maximum Hertzian pressures are higher than the indentation hardness, the asperity at the center will undergo plastic deformation. If the boundary between the plastic and elastic deformation is taken as though the top pressure has been truncated at a level corresponding

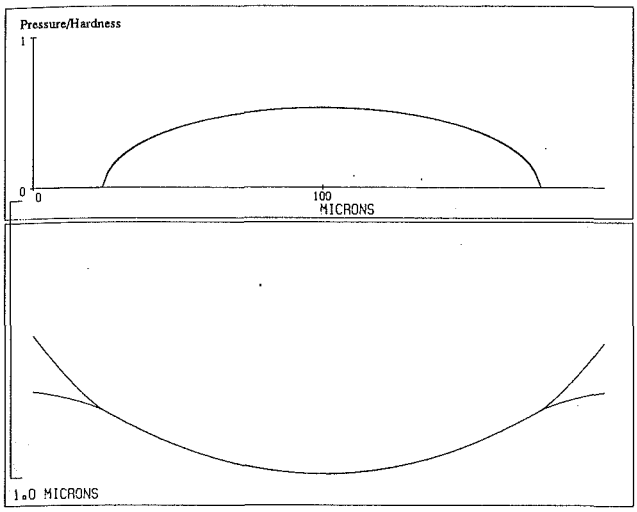

Fig. 7 Smooth case results from the numerical contact model. A Hertzian pressure distribution has been superimposed and is seen to correspond almost exactly to the numerical results. $p_n = 0.56$ Gpa, $H = 160$ H_v, $E_1 = E_2 = 207$ Gpa, $\nu_1 = \nu_2 = 0.3$.

to the hardness of the softer material, the plastic contact width based upon the geometrical overlap is likely to be overestimated. Should this happen, the numerical program may crash or have problems with convergence.

The problem can be avoided by decreasing the maximum pressure in stages. The intermediate hardness can be taken as two or three times the actual hardness such that the pressures higher than the intermediate hardness are reduced until all contact assumptions are satisfied.

The complete solution for a given load and geometry is obtained as follows and a flow chart showing the major features of the solution is shown in Fig. 6.

Step 1 Setup constants

Values δ, E_1, E_2, v_1, v_2, ball diameter, contact position and total load are input by the operator through the VDU.

Step 2 Setup geometry

Read data from files of either previously recorded surface profiles, or generated from appropriate body shapes stored in variable arrays. Then calculate sphere coordinates in relation to the profile.

Step 3 Rigid body movement

The upper body is given a rigid body displacement δ toward the lower body until contact is detected.

Step 4 Setup Matrices for first iteration

Values of u_i and C_{ij} are calculated for all overlapped points using Eqs. (6) and (15), respectively. w_j's are calculated from the geometrical overlap. An index array is used to store the positions of the contacting elements, which is then used to calculate the values of x by Eq. (12) and check for recontact. The surface displacement points are set at the center of contact.

Step 5 Solve for pressures

Solve for values of p_j's for the current displacement, using Gaussian Elimination.

Step 6 Check for negative pressures

The solution for p_j can give some negative (tensile) pressures which therefore violates assumption 3. This is due to the fact that the initial guess at δ_i, based upon the geometric overlaps, contains points which will not be part of the true solution and hence underestimates the true surface strains. A new set of u_i's are then calculated, but excluding points corresponding to $p_j < 0$. A second array is used to store the position of the current contacting elements and is used to calculate the new C_{ij} values. Steps 4, 5, and 6 are repeated until all p_j's > 0.

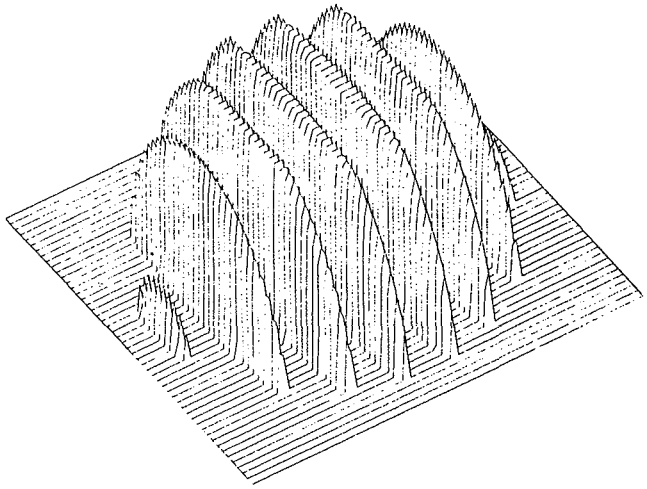

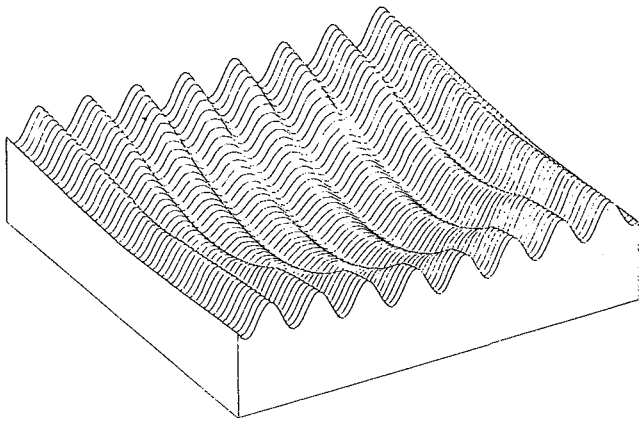

Fig. 8 (*a*) Three-dimensional view

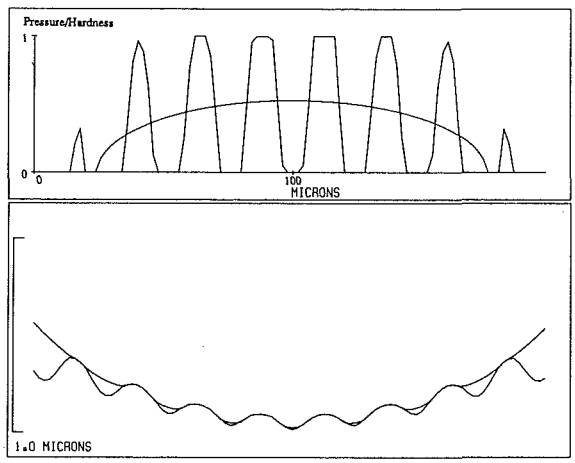

Fig. 8 (*b*) At a section through the center

Fig. 8 Pressure distribution and deformed geometry of a ball on a sinusoidal surface using the numerical contact model. $p_n = 0.56$ Gpa, $H = 160$ H_v, $E_1 = E_2 = 207$ Gpa, $\nu_1 = \nu_2 = 0.3$, $\Delta = 0.08$ μm, $\lambda = 24$ μm, Ball diameter = 12.7 mm.

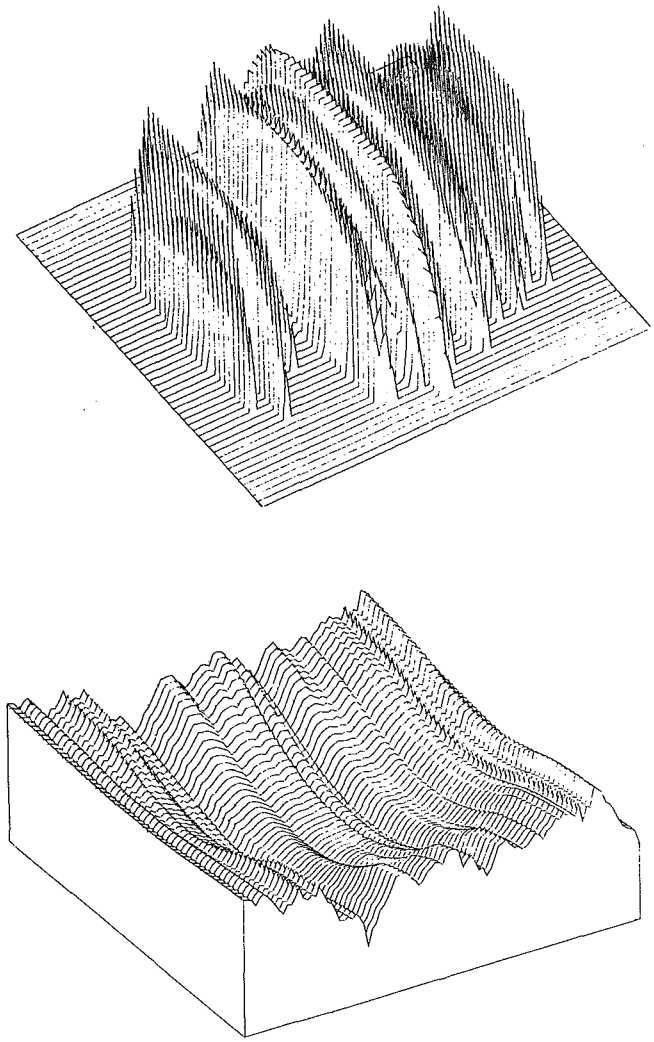

Fig. 9 (*a*) Three-dimensional view

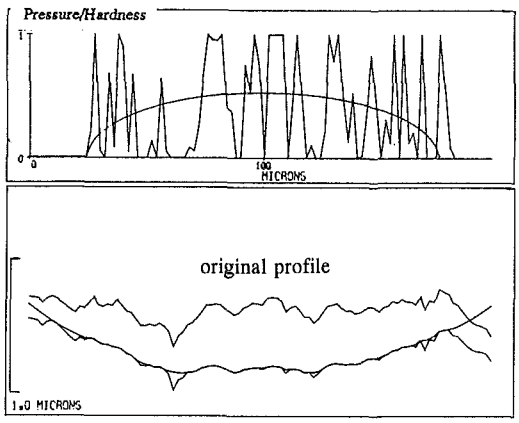

Fig. 9 (*b*) At a section through the center

Fig. 9 Pressure distribution and deformed geometry of a ball on a rough surface using the numerical contact model. $p_n = 0.56$ Gpa, $H = 160$ H_v, $E_1 = E_2 = 207$ Gpa, $\nu_1 = \nu_1 = 0.3$, $\sigma = 0.07$ μm, $\beta = 7.4$ μm, ball diameter = 12.7 mm.

Step 7 Setup intermediate hardness

It is necessary to reduce the plastic pressure in stages in avoid problems with convergence. The intermediate stages are set at $p_s = 1.5H, 2.0H, 2.5H, 3.0H$, and so on. Therefore, the number of stages depends on the maximum pressure calculated. Any asperity contact with $p_j > p_s$ is subjected to an increase in its plastic contact width until all p_j's $< p_s$.

Step 8 Calculate plastic contact width, checking recontact or calculate contact length

The calculation of plastic contact width, number of contacts and contact length are obtained individually while keeping the others as constants. A sequence is set up to reduce first the plastic pressure to the immediate hardness. Then any p_j's < 0 or contact previously occurs in step 4 are checked for recontact outside geometrical overlapped contact boundary. Finally, the contact lengths are calculated using Eq. (31) until all the Δw_j's < 2 μm. An index NSEQ is set for the next operation after each set of calculations is finished.

Step 9 Reduce intermediate hardness

If the intermediate hardness p_s is greater than the indentation hardness H_s, the intermediate hardness is reduced according to step 7 for the next operation. Steps from 4 are repeated again until the intermediate pressure is reduced to the required hardness.

Step 10 Output data

Numerical integration of the elemental pressure, contact width and plastic contact width are performed to calculate the load, total contact area and plastic area, respectively. If the resulting pressure integral is less than the required total load, the process is repeated from step 4. Output data files are created to store load versus area results, pressures, and initial and final geometries.

Figure 7 shows a test case of the contact on a smooth surface. The theoretical pressure distribution and normal displacement are plotted on the same axis. The numerical result corresponds almost exact with the Hertz analytical result. Figure 8(*a*) shows a three-dimensional view of the pressure distribution and the deformed geometry of a ball on a sinusoidal profile. Figure 8(*b*) shows the pressure distribution and normal displacement at a section through the center. The results show the expected behavior, i.e., a number of contact regions in which the peak pressure is flattened by plastic deformation and decreases away from the ball center. Figure 9(*a*) shows a three-dimensional view of the pressure distribution and the deformed geometry of a smooth ball on a rough surface. Figure 9(*b*) shows the pressure distribution and the deformed profile at a section through the center. Such results indicate that the numerical contact model described represents a very useful tool for investigating the problems of rough surface contact.

Due to the assumptions that the surface height varies only in the x-direction, the present approach is restrictive to the contact of a ball on a directionally rough surface. However, there are many engineering surfaces such as produced by grinding, turning, milling in which the surface roughness are strongly directionally structured and the surface height variation in one direction is much larger than the other direction. The two-dimensional contact model can be applied to study the contact problems of these surfaces. There are certain advantages of using the present approach. First, in the contact model, only one single roughness profile is used and thus eliminating the effort to perform three dimensional rough surface measurement. Second, due to the contact is two dimensional, the computing cost can be greatly reduced.

References

Bentall, R. H., and Johnson, K. L., 1967, "Slip in the Rolling Contact of Two Dissimilar Elastic Rollers," *Int. J. Mech. Sci.*, Vol. 9, p. 389.

Boussinesq, J., 1885, "Application des potentials a l'etude de l'equilibre et du mouvement des solids elastique," Gauthier-Villars, Paris.

Bowden, F. P., and Tabor, D., 1950, "The Friction and Lubrication of Solids, Part 1," Oxford University Press.

Cerruti, V., 1882, "Roma, Acc. Lincei," Mem. fis. mat.

Bush, A. W., Gibson, R. D., and Thomas, T. R., 1975, "The Elastic Contact of a Rough Surfaces," *Wear*, Vol. 35, pp. 87–111.

Bush, A. W., Gibson, R. D., and Keigh, G. P., 1976, "The Limit of Elsatic Deformation in the Contact of Rough Surfaces," *Mech. Res. Comm.*, Vol. 3, pp. 169–174.

Bush, A. W., Gibson, R. D., and Keogh, G. P., 1977, "Strongly Anisotropic Rough Surfaces," ASME JOURNAL OF LUBRICATION TECHNOLOGY, Jan., Vol. 101, pp. 15–20.

Chiu, Y. P., and Liu, J. Y., 1970, "An Analytical Study of the Stress Concentration around a Furrow Shaped Surface Defect in Rolling Contact," ASME JOURNAL OF LUBRICATION TECHNOLOGY, Vol. 92, pp. 258–263.

Dyson, J., and Hirst, W., 1954, "The True Contact Area Between Solids," *Proc. Phys. Soc. Lond.*, Series 67B, pp. 309–312.

Francis, H. A., 1982, "A Finite Surface Element Model for Plane-Strain Elastic Contact," *Wear*, Vol. 76, pp. 221–245.

Francis, H. A., 1983, "The Accuracy of Plane-Strain Models for the Elastic Contact of Three-Dimensional Rough Surfaces," *Wear*, Vol. 85, pp. 239–256.

Greenwood, J. A., and Williamson, J. B. P., 1966, "Contact of Nominally Flat Surfaces," *Proc. Roy. Soc. Lond.*, Series A295, pp. 300–319.

Hirst, W., and Hollander, A. E., 1974, "Surface Finish and Damage in Sliding," *Proc. Roy. Soc. Lond.*, Series A337, pp. 379–394.

Holm, R., 1958, *Electric Contacts Handbook*, Springer-Verlag, Berlin.

Johannet, P., 1972, "Study of Internal Structure of Closed Contacts under Load by a Neutrographic Method," *Proc. 6th Conf. Electric Contact Phenomena*, 11T, Illinois Instn. Technol., Chicago.

Johnson, K. L., 1985, *Contact Mechanics*, Cambridge University Press.

Kalker, J. J., and Van Randen, Y., 1972, "A Minimum Principle for Frictionless Elastic Contact With Application to Non-Hertzian Half-Space Contact Problems," *J. Engng. Maths.*, Vol. 6, p. 193.

Kragelskii, J. V., 1965, *Friction and Wear*, Butterworths, London.

Kragelskii, J. V., and Demkin, N. B., 1960, "Determination of the True Contact Area," *Friction Wear Mach* (USSR), Vol. 14, p. 30.

Longuet-Higgins, M. S., 1957a, "The Statistical Analysis of a Random Moving Surface," *Phil. Trans. Roy. Soc.*, Series A249, pp. 321–387.

Longuet-Higgins, M. S., 1957b, "Statistical Properties of an Isotropic Random Surface," *Phil. Trans. Roy. Soc.*, Series A250, pp. 157–174.

Love, A. E. H., 1929, "The Stress Produced in a Semi-Infinite Solid by Pressure on Part of the Boundary," *Proc. Roy. Soc. Lond.*, Series A228, p. 377.

Love, A. E. H., 1952, *A Treatise on the Mathematical Theory of Elasticity*, 4th edition, Cambridge University Press.

Mikic, B. B., and Roca, R. T., 1974, "Thermal Contact Conductance; Theoretical Considerations," *Int. J. Heat and Mass Transfer*, Vol. 17, pp. 205–214.

Mulhearn, T. O., 1959, "Deformation of Metals by Vickers Type Pyramidal Indenters," *J. Mech. and Phys. of Solids*, Vol. 7, p. 85.

Nayak, P. R., 1971, "Random Process Model of Rough Surfaces," ASME JOURNAL OF LUBRICATION TECHNOLOGY, Vol. 93, pp. 398–407.

Onions, R. A., and Archard, J. F., 1973, "The Contact of Surfaces Having a Random Structures," *J. Phys. D: Applied Phys.*, Vol. 6, pp. 289–304.

Paul, B., and Hashemi, J., 1981, "Contact Pressure on Closely Conforming Elastic Bodies," ASME *Journal of Applied Mech.*, Vol. 48, p. 543.

Poon, C. Y., 1989, "Frictional Transition in Boundary Lubrication Sliding," 2nd Int. Conf. on Combustion Engines-Reduction of Friction and Wear, IMechE, London, Sept. 1989.

Poon, C. Y., 1990, "The Influence of Surface Topography on Sliding Friction in Boundary Lubrication," PhD Thesis, Imperial College, London.

Samuels, L. E., and Mulhearn, T. O., 1956, "The Deformed Zone Associated with Indentation Hardness Impressions," *J. Mech. and Phys. of Solids*, Vol. 5, p. 125.

Sayles, R. S., and Thomas, T. R., 1978b, "Computer Simulation of the Contact of Rough Surfaces," *Wear*, Vol. 49, pp. 273–296.

Suratkar, P. T., Pandit, S. M., and Wu, S. M., 1976, "A Stochastic Approach to the Mode of Deformation and Contact Between Rough Surfaces," *Wear*, Vol. 39, pp. 239–250.

Tsukizoe, T., and Hisakado, T., 1965, "On the Mechanism of Contact Between Metal Surfaces—The Penetrating Depth and the Average Clearance," ASME JOURNAL OF LUBRICATION TECHNOLOGY, Sept., pp. 666–674.

Tsukizoe, T., and Hisakado, T., 1968, "On the Mechanism of Contact Between Metal Surface: Part 2—The Real Area and the Number of the Contact Points," ASME JOURNAL OF LUBRICATION TECHNOLOGY, Jan., pp. 81–88.

Uppal, A. H., and Probert, S. D., 1973, "Mean Separation and Real Contact Area Between Surfaces Pressed Together Under High Static Loads," *Wear*, Vol. 23, pp. 39–53.

Uppal, A. H., Probert, S. D., and Thomas, T. R., 1972, "The Real Area of Contact Between a Rough and a Flat Surface," *Wear*, Vol. 22, p. 163.

Webster, M. N., and Sayles, R. S., 1986, "A Numerical Model for the Elastic Frictionless Contact of Real Rough Surfaces," ASME JOURNAL OF TRIBOLOGY, Vol. 108, pp. 314–320.

West, M. A., and Sayles, R. S., 1987b, "A 3-Dimensional Method of Studying 3-Body Contact Geometry and Stress on Real Rough Surfaces," *The 14th Leeds Lyon Symposium, "Interface Dynamics."*

West, M. A., Webster, M. N., and Sayles, R. S., 1987a, "A New Method for Rough Surface Contact Analysis," *Proc. Instn Mech. Engrs., Tribology—Friction, Lubrication and Wear, Fifty Years*, pp. 945–955.

Williamson, J. B. P., 1967/68, "The Microtopography of Surfaces," *Proc. Instn. Mech. Engrs.*, Vol. 182, part 3k, pp. 21–30.

Williamson, J. B. P., and Hunt, R. T., 1968, "Relocation Profilometry," *J. Instsn. Phys*, Series E, Scientific Instruments 2, Vol. 1, p. 749.

APPENDIX

The total surface displacement u_i due to the pressure acting at j is given by Eq. (23).

$$u_i = \frac{1-v^2}{\pi E} \sum_j \sum_k p_j \alpha_k F_{xy} \tag{A1}$$

Differentiate Eq. (A1) with respect to w_j,

$$\frac{du_i}{dw_j} = \frac{1-v^2}{\pi E} \sum_j p_j \sum_k \alpha_k F'_{xy} + \frac{1-v^2}{\pi E} \sum_j p_j' \sum_k \alpha_k F_{xy} \tag{A2}$$

At the boundary of contact, Eq. (9) can be used as a good approximation, i.e.,

$$F_{xy} = \frac{2a \cdot 2b}{\sqrt{x^2+y^2}} \tag{A3}$$

b and y are function of w_j and are given by,

$$b = \mu w_j / 2 \tag{A4}$$

and

$$y = \mu k w_j \quad \text{where} \quad \mu = 2/(2N_y + 1) \tag{A5}$$

Differentiate Eq. (A3) with respect to w_j, and using Eqs. (A4) and (A5),

$$F'_{xy} = \frac{2a\,\mu(x^2+y^2-\mu k w_j y)}{(x^2+y^2)^{3/2}}$$

$$= \frac{2a\mu x^2}{(x^2+y^2)^{3/2}} \tag{A6}$$

Substitute Eqs. (A3) and (A6) into Eq. (A2),

$$\frac{du_i}{dw_j} = \frac{2a(1-v^2)}{\pi E} \sum_j p_j \sum_k \alpha_k \frac{\mu x^2}{(x^2+y^2)^{3/2}} + \frac{2a(1-v^2)}{\pi E} \sum_j \frac{dp_j}{dw_j} \sum_k \alpha_k \frac{\mu w_j}{(x^2+y^2)^{1/2}} \tag{A7}$$